Eur. Phys. J. B **12**, 261–268 (1999)

THE EUROPEAN PHYSICAL JOURNAL B

EDP Sciences

Phase diagram of magnetic polymers

T. Garel[1], H. Orland[1,a], and E. Orlandini[2]

[1] Service de Physique Théorique, CEA Saclay, 91191 Gif-sur-Yvette Cedex, France
[2] Istituto Nazionale per la Fisica della Materia (INFM) and Dipartimento di Fisica dell'Universita' di Padova, via Marzolo 8, 35131 Padova, Italy

Received 11 February 1999

Abstract. We consider polymers made of magnetic monomers (Ising or Heisenberg-like) in a good solvent. These polymers are modeled as self-avoiding walks on a cubic lattice, and the ferromagnetic interaction between the spins carried by the monomers is short-ranged in space. At low temperature, these polymers undergo a magnetic induced first order collapse transition, that we study at the mean field level. Contrasting with an ordinary Θ point, there is a strong jump in the polymer density, as well as in its magnetization. In the presence of a magnetic field, the collapse temperature increases, while the discontinuities decrease. Beyond a multicritical point, the transition becomes second order and Θ-like. Monte Carlo simulations for the Ising case are in qualitative agreement with these results.

PACS. 36.20.Ey Conformation (statistics and dynamics) – 64.70.-p Specific phase transitions – 75.50.-y Studies of specific magnetic materials

1 Introduction

Under various solvent conditions, a polymer chain can be either swollen or collapsed. In a bad solvent, a phase transition between these two states can occur as temperature is varied [1]. This is the so-called Θ point, the tricritical nature of which has been demonstrated by de Gennes [2]. The effective monomer-monomer attraction results from tracing out the solvent degrees of freedom. At the Θ point, the second virial coefficient of the polymer vanishes.

In this paper, we consider a different mechanism that also yields attractive monomer-monomer interactions. The model we study consists of a polymer chain, where each monomer carries a spin S in an external magnetic field; these spins interact with each other with a short-ranged interaction. To be specific, we will consider a self-avoiding walk (SAW) of length N, on a d-dimensional cubic lattice, with a nearest-neighbor ferromagnetic interaction (on the lattice) between the spins of the monomers.

Several models involving both polymeric and magnetic-like degrees of freedom have been introduced in very different contexts. A similar, but somewhat more complicated model, was studied to describe secondary structure formation in proteins [3]: there, the dominant interactions between the monomers are of (electric) dipolar nature. A Potts model on a SAW was studied as a description of vulcanization in [4]; a similar model with quenched disorder was studied in the context of secondary structure formation in proteins [5].

Ising models have also been studied on a fixed SAW geometry, yielding results quite different from those presented here [6,7]. From an experimental point of view, organic polymeric magnets have recently become of interest [8,9]. However, there has been very little interest in their conformational changes.

In the following, we will specialize to the Ising case, and quote some results for the Heisenberg case. The partition function of the system reads:

$$Z = \sum_{\mathrm{SAW}} \sum_{S_i=\pm 1} \exp\left(\frac{\beta J}{2} \sum_{i \neq j} S_i \Delta_{r_i r_j} S_j + \beta h \sum_i S_i \right) \tag{1}$$

where J is the exchange energy, $\beta = \frac{1}{T}$ the inverse temperature, and h the external magnetic field. The spatial position of monomer i with spin S_i is r_i. The symbol $\Delta_{rr'}$ is 1 if $\{r, r'\}$ are nearest-neighbor on the lattice and 0 otherwise. The sums run over all possible SAW and all spin configurations.

This model will be studied along three lines. In Section 2, we derive upper bounds for the free energy of the model (in zero magnetic field) which suggest a first order transition between a swollen paramagnetic and a collapsed magnetized phase. In Section 3, we derive a mean-field theory for the general model. We show that indeed for low fields, there is a such a line of first-order transitions. At higher fields, this transition becomes continuous. The two regimes are separated by a multicritical G point. At this special point, both the second and the third virial coefficient vanish. In Section 4, these predictions are tested

[a] e-mail: orland@spht.saclay.cea.fr

against Monte Carlo simulations in $d = 3$ dimensions. The numerical results are consistent with the theoretical phase diagram; at low field (where the transition is strongly first order), the agreement is even quantitative.

2 Free energy bounds

The physics of the model can be described according to the following simple picture.

1. At high temperature, since entropy dominates, the chain is swollen. As a result, the number of nearest-neighbor contacts is small, and from a magnetic point of view, the system is equivalent to a one-dimensional Ising model. This simple picture can be expressed through the following inequality:

$$Z \geq Z_{\mathrm{SAW}} Z_1(h) \tag{2}$$

where Z_{SAW} is the total number of SAW, and $Z_1(h)$ is the partition function of the one-dimensional Ising model in a field h. Using well known results [10,11]:

$$Z_{\mathrm{SAW}} \sim \mu^N N^{\gamma-1} \tag{3}$$

where γ is a critical exponent, we obtain:

$$\frac{F}{N} \leq -T \log \mu - T \log(\mathrm{e}^{\beta J} \cosh \beta h + \sqrt{\mathrm{e}^{2\beta J} \sinh^2 \beta h + \mathrm{e}^{-2\beta J}}). \tag{4}$$

The best estimate in $d = 3$ is $\mu \simeq 4.68$ for the cubic lattice [12].

2. At low temperature, the magnetic energy is larger than the entropy loss due to confinement, and thus the chain collapses. The simplest picture is that of a totally magnetized and fully compact system, resulting in the following bound:

$$Z \geq \exp(N\beta J d + N\beta h)\ Z_{\mathrm{HP}} \tag{5}$$

where Z_{HP} is the entropy of Hamiltonian paths (HP) on the lattice, *i.e.* fully compact SAW on the lattice[1]. Using a virtually exact upper bound [13] to Z_{HP}, we obtain:

$$\frac{F}{N} \leq -T \log \frac{2d}{e} - Jd - h. \tag{6}$$

Note that in two dimensions and in zero magnetic field, it is possible to write a more accurate bound by using the exact expression Z_2 for the Onsager partition function of the Ising model:

$$Z \geq Z_2 Z_{\mathrm{HP}}. \tag{7}$$

The free energy bounds of equations (4, 6) are shown as functions of temperature in Figure 1, for $d = 3$ and $h = 0$. The true free energy lies below these two curves, and their intersection is an indication for a possible first order transition between the swollen and collapsed phases.

[1] A HP is a SAW which passes through each point of the lattice exactly once.

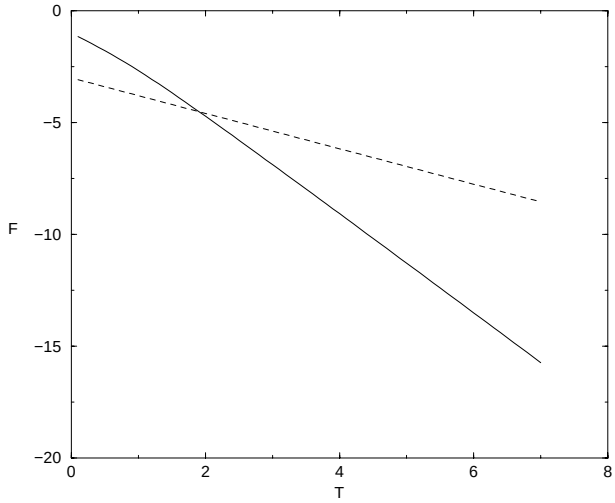

Fig. 1. The high temperature (solid line) and low temperature (dashed line) free energy bounds for $d = 3$ and $h = 0$.

3 Mean-field theory

By using a Gaussian transform, it is possible to write a field-theoretical representation for the model (1):

$$Z = 2^N \int \prod_r \mathrm{d}\varphi_r \exp\left(-\frac{1}{2\beta J} \sum_{\{r,r'\}} \varphi_r \Delta^{-1}_{r,r'} \varphi_{r'} + \log \sum_{\mathrm{SAW}\{r_i\}} \prod_{i=1}^{N} \cosh(\varphi_{r_i} + \beta h) \right). \tag{8}$$

As usually, the mean-field theory can be obtained by performing a saddle-point approximation on equation (8). We assume that the chain is confined in a volume V with a monomer density $\rho = \frac{N}{V}$. Assuming a translationally invariant field φ, the mean field free energy per monomer is

$$f = \frac{F}{N} = -T \log 2 + \frac{T^2}{2\rho J q} \varphi^2 - T \log Z_{\mathrm{SAW}} - T \log \cosh(\varphi + \beta h) \tag{9}$$

where $q = 2d$ is the coordination number of the cubic lattice and Z_{SAW} is the total number of SAW of N monomers confined in a volume V. Following reference [13], it is easily seen that:

$$Z_{\mathrm{SAW}} \simeq \left(\frac{q}{e}\right)^N \exp\big(-V(1-\rho)\log(1-\rho)\big) \tag{10}$$

so that

$$f = -T \log 2 + \frac{T^2}{2\rho J q} \varphi^2 - T \log \frac{q}{e} + T\, \frac{1-\rho}{\rho}\, \log(1-\rho) - T \log \cosh(\varphi + \beta h). \tag{11}$$

This free energy is to be minimized with respect to the field φ and to the volume V occupied by the chain, or

equivalently to the monomer concentration ρ. The mean field equations read:

$$T\frac{\varphi^2}{2Jq} = -\rho - \log(1-\rho), \tag{12}$$

$$\varphi = \beta J \rho q \ \tanh(\varphi + \beta h). \tag{13}$$

Note that this free energy holds also for a melt of chains, where ρ is the total monomer concentration.

This set of coupled equations has a high temperature solution $\rho = 0$, $\varphi = 0$, which describes the swollen phase with no magnetization and vanishing monomer concentration, and a low temperature solution, which describes a collapsed phase with a finite monomer concentration and magnetization. More precisely, for magnetic fields $h < h_{\rm G}$, there is a first order transition (as a function of temperature) between a swollen and a collapsed phase. At higher fields $h > h_{\rm G}$, the transition becomes second order (in fact tricritical). For infinite fields, the magnetization saturates, and the model becomes equivalent to the ordinary Θ point as studied in many papers [14–16].

Expanding (12) and (13), one obtains the equation for the second order line:

$$\tanh \beta h = \sqrt{\frac{T}{Jq}}\,. \tag{14}$$

Close to this critical line, the concentration varies as:

$$\rho \sim \frac{1}{2}\frac{1 - \beta Jq \tanh^2 \beta h}{(\beta Jq)(1-\tanh^2 \beta h) - \frac{1}{3}} \tag{15}$$

and the magnetization per spin is given by

$$M \sim \tanh \beta h \tag{16}$$

and remains finite, whereas the magnetization per unit volume, given by

$$m \sim \rho \tanh \beta h \tag{17}$$

vanishes.

The phase diagram is shown in Figure 2, with values corresponding to dimension $d = 3$.

The first order and continuous transitions are separated by a multicritical point, denoted by G in Figure 2. The corresponding temperature and field are $T_{\rm G} = 4.5J$ and $h_{\rm G} = 5.926J$. At zero magnetic field (point A), the transition temperature is $T_{\rm c} = 1.886J$, the critical concentration is $\rho_{\rm c} = 0.87$ and the critical magnetization per unit volume is $m_{\rm c} = 0.87$. Note that the magnetic susceptibility $\chi = \partial M/\partial h$ remains finite along the second order critical line.

The same phase diagram holds for the Heisenberg ferromagnet, with a multicritical G point at $T_{\rm G} = 2.31J$, $h_{\rm G} = 5.91J$. The zero-field point A is at $T_{\rm c} = 0.844J$, $\rho_{\rm c} = 0.902$ and $m_{\rm c} = 0.73$.

Using (13) to eliminate φ as a function of ρ, it is possible to express the free energy (11) only as a function of the monomer concentration ρ. This yields the virial expansion of the free energy. The second virial coefficient vanishes along the second order line (14), implying that the transition is Θ-like (*i.e.* tricritical). At the multicritical G point, both the second and third virial coefficients vanish, while the fourth order coefficient is positive.

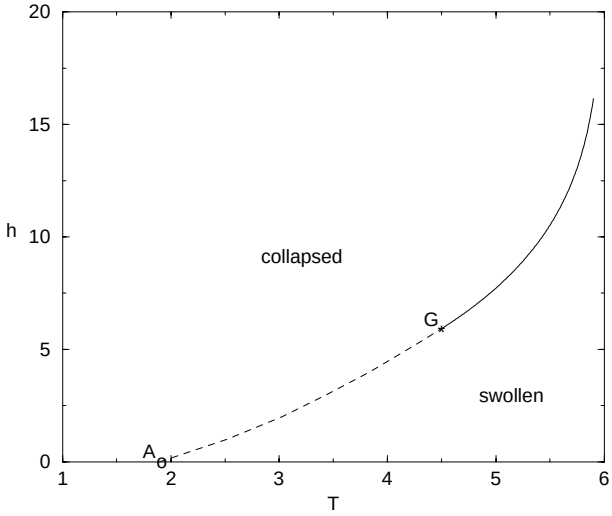

Fig. 2. Mean-field phase diagram in $d = 3$ for Ising spins. The dashed line corresponds to a first order transition, and the solid line to a second order (Θ-like) transition.

4 Monte Carlo simulations

The Monte Carlo method [17] used to compute thermodynamic as well as geometric properties of the magnetic chain relies on the multiple Markov chain sampling. A detailed description of this method can be found in [16,18]. The implementation we consider for a magnetic chain on a three-dimensional cubic lattice, can be summarized as follows.

We start from a single Markov chain at fixed temperature T. The probability $\pi_{\mathcal{D}}(T)$ of a (magnetic) chain configuration $\mathcal{D}$, is given by the Boltzmann distribution $\pi_{\mathcal{D}}(T) \sim {\rm e}^{-H(\mathcal{D})/T}$ with

$$H(\mathcal{D}) = -\frac{J}{2}\sum_{i\neq j} S_i \Delta_{r_i r_j} S_j - h\sum_i S_i \tag{18}$$

where the thermodynamic variables S_i and r_i are assigned their $\mathcal{D}$-dependent values. This Markov chain is generated by a Metropolis heath bath sampling based on a hybrid algorithm for chains with pivot [19] a well as local moves [20]. Pivot moves are nonlocal moves that assure the ergodicity of the algorithm; they operate well in the swollen phase but their efficiency deteriorate close to the compact phase. In this respect local moves become essential to speed up the converge of the Markov chain. Finally, in addition to the moves that deform the chain, an algorithm based on Glauber dynamics is considered to update the spin configuration along the chain. For a single Markov chain we typically consider $\sim 10^6$ pivot moves intercalated by $N/4$ local moves and N spin updates.

The multiple Markov chain algorithm is then implemented on the hybrid algorithm described above. The idea is to run in parallel a number p (in this work $p = 20-25$) of Markov chains at different temperatures $T_1 > T_2 > \cdots > T_p$. In practice, this set of temperatures is such that the configurations at T_j and at T_{j+1} have considerable overlap (implying that T_j and T_{j+1} are close enough). We let the Markov chains interact by possibly exchanging configurations as follows. Two neighboring Markov chains (*i.e.* with temperatures T_j and T_{j+1}) are selected at random with uniform probability. A trial move is an attempt to swap the two current configurations of these Markov chains. If we denote by $\pi_K(T)$ the Boltzmann probability of getting configuration K at temperature T, and $\mathcal{D}_j$ and $\mathcal{D}_{j+1}$ the current states in the jth and $(j+1)$th Markov chain, then we accept the trial move (*i.e.* swap $\mathcal{D}_j$ and $\mathcal{D}_{j+1}$) with probability

$$r(\mathcal{D}_j, \mathcal{D}_{j+1}) = \min\left(1, \frac{\pi_{\mathcal{D}_{j+1}}(T_j)\pi_{\mathcal{D}_j}(T_{j+1})}{\pi_{\mathcal{D}_j}(T_j)\pi_{\mathcal{D}_{j+1}}(T_{j+1})}\right). \quad (19)$$

The whole process is itself a (composite) Markov chain that is ergodic, since the underlying Markov chains are themselves ergodic. It turns out that the swapping procedure dramatically decreases the correlation times within each Markov chain with little cost in CPU time since, in any case, one is interested in obtaining data at many temperatures [16,18].

For each multiple Markov chain run we compute estimates, at a discrete set of temperatures T, of quantities such as (i) the average energy $\langle \mathcal{E} \rangle$ and specific heat $\mathcal{C} = \frac{\langle \mathcal{E}^2 \rangle - \langle \mathcal{E} \rangle^2}{T^2}$ of the chain. The per monomer quantities will be denoted respectively by E and C (ii) the average magnetization per monomer $M = \frac{1}{N}\sum_i \langle S_i \rangle$ (iii) the susceptibility $\chi = \frac{\partial M}{\partial h}$. In addition, as a geometric quantity, we consider the mean squared radius of gyration $\langle R^2 \rangle$ of the chain. From now on, we will set $J = 1$, which amounts to give the values of the field and temperature in units of J.

We have done preliminary simulations at high ($T = 10$) and low ($T = 1$) temperature. Our results (Fig. 3) show that the chain undergoes a swollen to collapsed phase transition, in broad agreement with the mean field picture; moreover, the radius of gyration is found to vary very little with the magnetic field (note that mean field theory yields $\rho_c = 0.87$ at T_c in zero field). Since a full exploration of the (h, T) plane is difficult, we have restricted this paper (i) to a detailed study of the $h = 0$ transition (ii) to a qualitative study of some non zero magnetic field transitions. As mentionned above, the infinite field case corresponds to the usual Θ situation: equation (14) then yields $T_\theta = q = 6$, whereas the experimental (cubic lattice) value is $T_\theta \simeq 3.7$ [15]. As expected in the presence of fluctuations, the mean field parameters (including the location of point G) are not reliable. For small h, the first order character of the mean field transition will be seen to improve the situation.

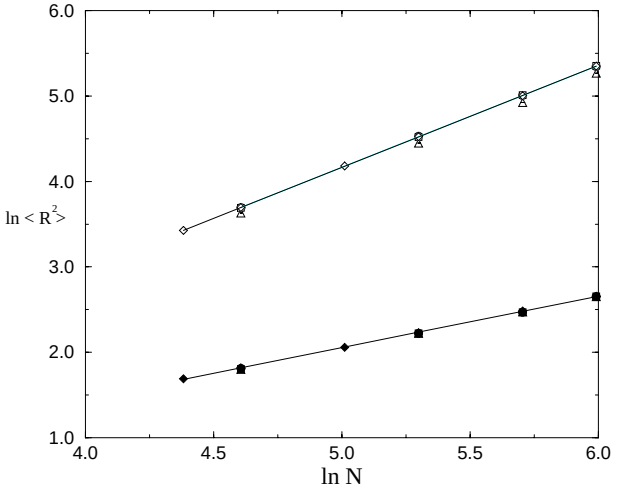

Fig. 3. Log-Log plot of $\langle R^2 \rangle$ *vs.* N, for $N = 80, 100, 150, 200, 300, 400$. The empty and filled symbols correspond respectively to $T = 10$ and $T = 1$. Values of the magnetic field are $h = 0$ ($\diamond$), 0.5 ($\circ$), 1 ($\square$) and $h = 10$ ($\triangle$). The lines have respective slope $2\nu = 1.194 \pm 0.005$ and $2\nu = 0.63 \pm 0.04$.

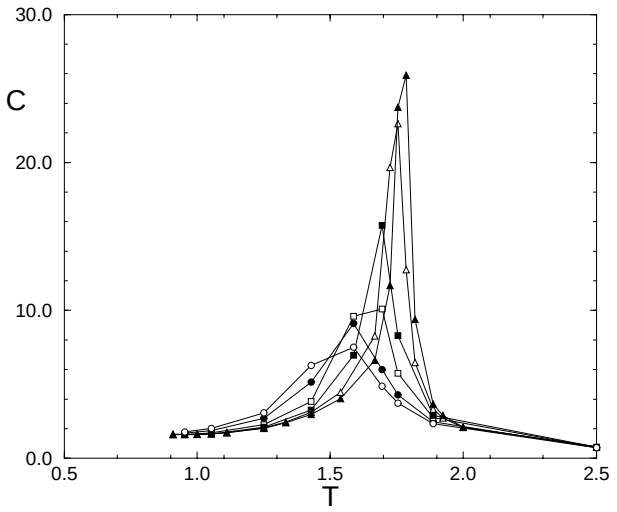

Fig. 4. Specific heat per monomer *vs.* temperature for $h = 0$ and $N = 80$ ($\circ$), 100 ($\bullet$), 150 ($\square$), 200 ($\blacksquare$), 300 ($\triangle$), 400 ($\blacktriangle$). Note the increase of the peak as well as its shape, when N increases.

4.1 Results for h = 0: Evidence for a first order transition

Our results for the specific heat per monomer C and the susceptibility χ are respectively given in Figures 4 and 7. The spiky character of both contrasts with the rounded specific heat of a usual Θ point. Indeed, finite size scaling theory [21] predicts that the peak $C_{\max}$ of the specific heat behaves, in the critical region (*i.e.* for large enough N), as

$$C_{\max} \sim N^{\frac{\alpha}{2-\alpha}} \quad (20)$$

where α is the critical exponent associated with the temperature divergence of the specific heat. Accordingly,

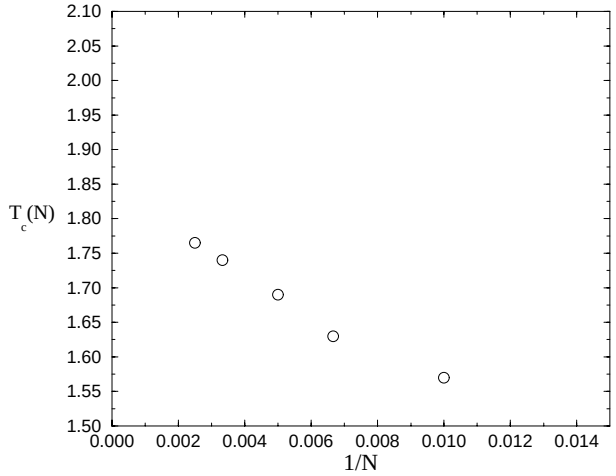

Fig. 5. Temperature location of the specific heat peak *vs.* $1/N$, for $N = 100,\ 150,\ 200,\ 300,\ 400$.

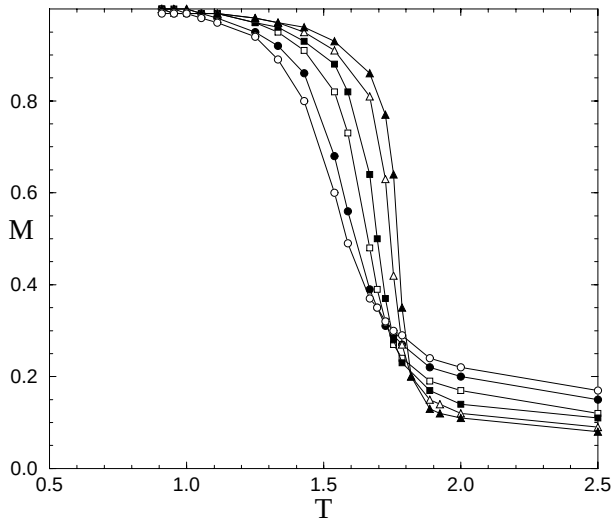

Fig. 6. Magnetization per spin *vs.* temperature for $h = 0$ and $N = 80$ (○), 100 (●), 150 (□), 200 (■), 300 (△), 400 (▲).

the critical temperature shifts from its $N = \infty$ value by an amount ΔT given by

$$\Delta T \sim N^{-\frac{1}{2-\alpha}}. \tag{21}$$

At the Θ point, one has $\alpha = 0$, implying a slow (logarithmic) N dependence of $C_{\max}$ and $\Delta T \sim \frac{1}{N^{1/2}}$ (up to a logarithmic factor). On the contrary, a thermal first order transition corresponds to the value $\alpha = 1$, yielding $C_{\max} \sim N$ with a much weaker temperature shift $\Delta T \sim \frac{1}{N}$. These scaling predictions are to be compared with the results of Figures 5 and 12. The agreement is satisfactory, even though it is not clear that the largest N value, *viz.* $N = 400$, is already in the scaling region. Further evidence for a discontinuous zero field transition comes from Figures 6 and 8, where we show the thermal evolution of the average magnetization per monomer M and of the radius of gyration. All these results are consistent with a first order transition at a critical temperature

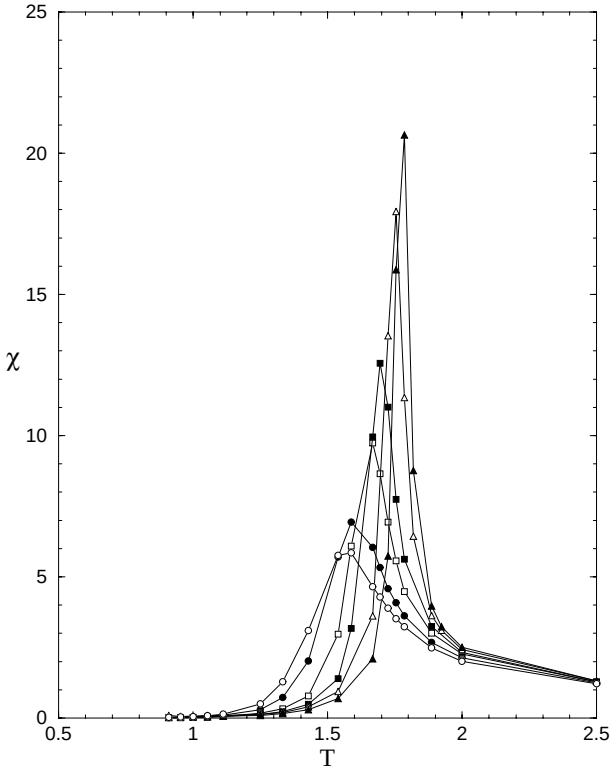

Fig. 7. Susceptibility *vs.* temperature for $h = 0$ and $N = 80$ (○), 100 (●), 150 (□), 200 (■), 300 (△), 400 (▲).

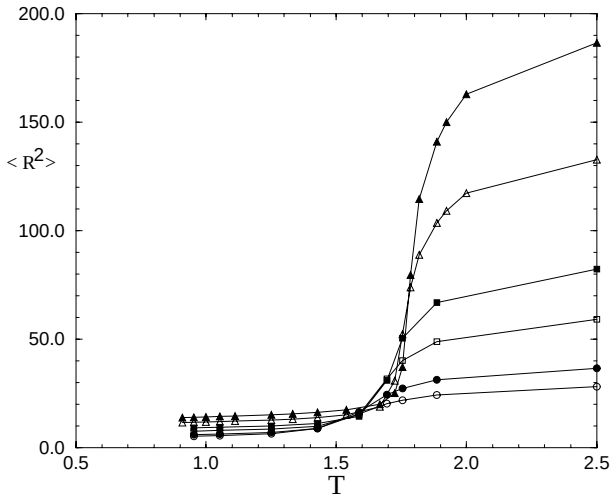

Fig. 8. Squared radius of gyration of the polymer as a function of temperature for $h = 0$, and $N = 80$ (○), 100 (●), 150 (□), 200 (■), 300 (△), 400 (▲).

$T_c \simeq 1.80 \pm 0.04$, close indeed to the mean field value $T_c^{MF} \simeq 1.88$.

To study the phase coexistence implied by such a transition, we have studied the probability distributions of the magnetization M and internal energy E close to the phase transition. Figures 9 and 10, obtained for $N = 300$, suggest that the critical distributions $P(M)$ and $P(E)$ are flat, in marked contrast with the usual two peak structure at T_c [22]. This two peak structure results

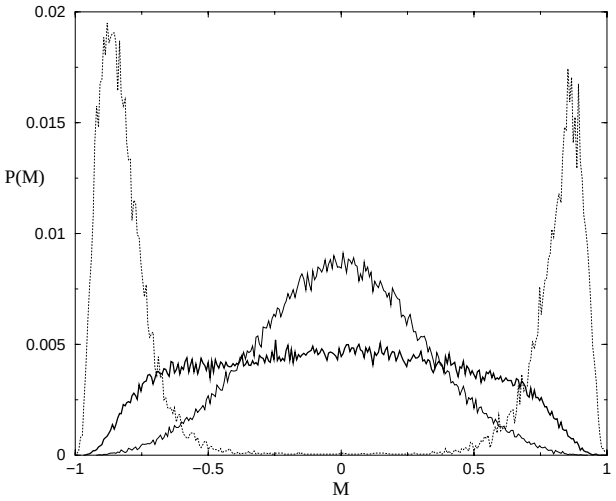

Fig. 9. Probability distribution $P(M)$ of the magnetization per monomer, for three different temperatures at $h = 0$ and $N = 300$: $T = 1.67 < T_c(N)$ dotted line, $T = 1.81 > T_c(N)$ solid line, $T = 1.78 \simeq T_c(N)$ thick line.

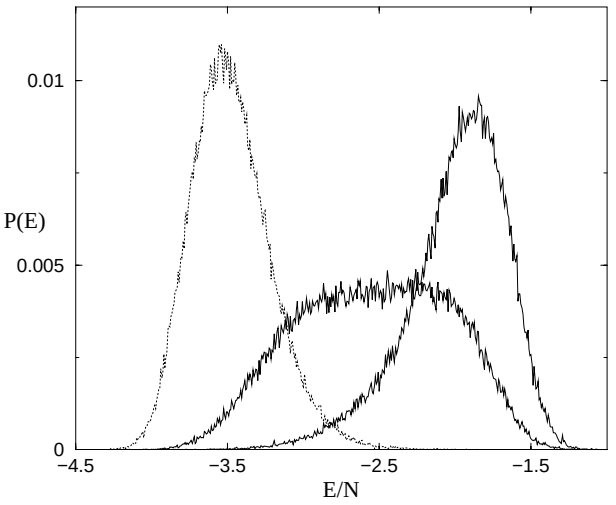

Fig. 10. Probability distribution $P(E)$ of the internal energy per monomer for three different temperatures at $h = 0$ and $N = 300$: $T = 1.67 < T_c(N)$ dotted line, $T = 1.81 > T_c(N)$ solid line, and $T = 1.78 \simeq T_c(N)$ thick line.

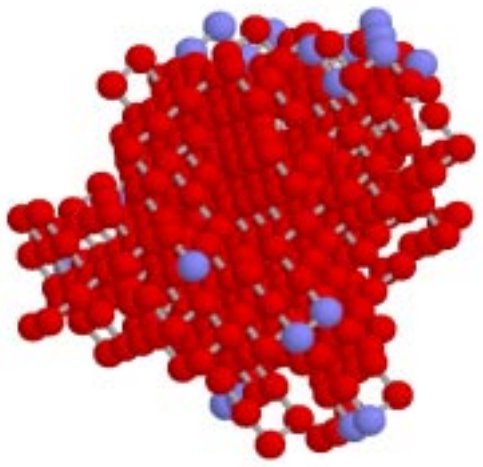

Fig. 11. Typical chain configuration just below the transition ($T = 1.65$), for $h = 0$. Dark grey (resp. light grey) monomers have up (resp. down) spins. Note that the down spins are on the surface of the globule.

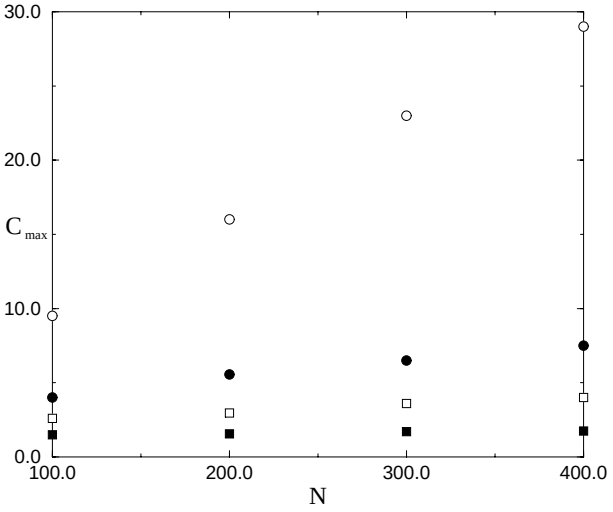

Fig. 12. Peak of the specific heat per monomer *vs.* N for different values of h: $h = 0$ (○), 0.5 (●), 1 (□), 10 (■). For $h = 10$, the value of $C_{\max}$ is clearly not proportional to N.

from the spatial coexistence of the (bulk) phases along a domain wall (more generally a $(d-1)$ interface). In the present case, we have coexistence between phases of different dimensionalities, namely a paramagnetic swollen phase and a magnetized collapsed phase. It is then clear that the "interface" can be reduced to a point, yielding a "surface" tension of order one. This in turn explains the flat critical distributions of Figures 9 and 10. Below the transition, it is interesting to note that the magnetization quickly saturates: a closer look at compact chain magnetic conformations shows that the minority domains are located on the surface of the globule, and become less and less relevant as N grows (Fig. 11).

4.2 Tentative studies of the continuous transition in a field

As previously mentionned, the multicritical point G will be pushed downwards from its mean field location. Since the computer search for a precise determination of this point is very time consuming, we have adopted the following strategy. We have performed simulations for small ($h = 0.5$ and $h = 1$) and large ($h = 5$ and $h = 10$) magnetic field.

The first evidence for a second order transition in large fields comes from Figure 12, where the specific heat maximum for $h = 10$ behaves very differently from its

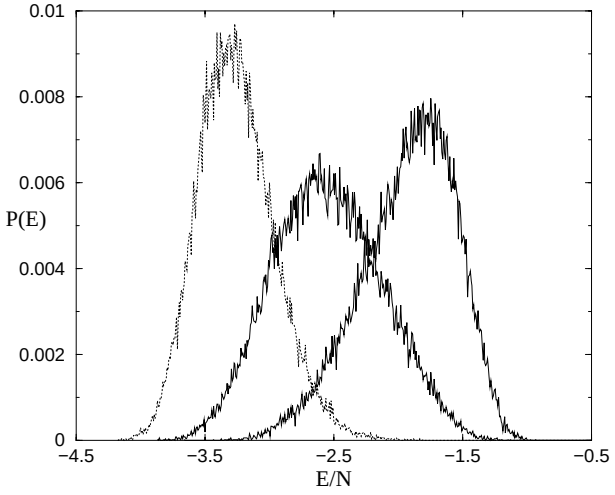

Fig. 13. Probability distribution $P(E)$ of the internal energy per monomer for three different temperatures at $h = 0.5$ and $N = 300$: $T = 1.74 < T_c(N)$ dotted line, $T = 1.89 > T_c(N)$ solid line, $T = 1.81 \simeq T_c(N)$ thick line.

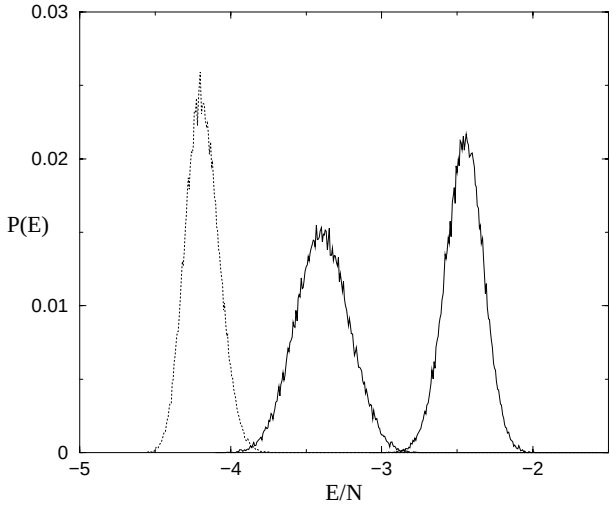

Fig. 14. Probability distribution $P(E)$ of the internal energy per monomer for three different temperatures at $h = 5$ and $N = 300$: $T = 1.67 < T_c(N)$ dotted line, $T = 4 > T_c(N)$ solid line, $T = 2.43 \simeq T_c(N)$ solid thicker line.

small field values: for $h = 0.5$ and $h = 1$, one apparently gets the same behaviour as with $h = 0$, namely $C_{\max} \sim N$. The existence of a second order transition for h large is corroborated by Figures 14 and 15. For $h = 5$, the critical probability distribution is very different from its $h = 0$ counterpart (Fig. 10). A finite size scaling analysis of the data for the same value of the field yields, in a rather convincing manner, a second order Θ like transition at $T_c \sim 3.4$ (remember that $\lim_{h\to\infty} T_c(h) \simeq 3.7$). We therefore obtain $h_G < 5$. To get a better estimate of h_G, we have computed the probability distribution $P(E)$ of the internal energy for $h = 0.5$ (Fig. 13). It clearly interpolates between Figures 10 and 14, but it is not easy to interpret the data as representative of a continuous or discontinuous transition. To summarize, we have presented evidence for a continuous transition for large h. The precise position of the point G is left for future work.

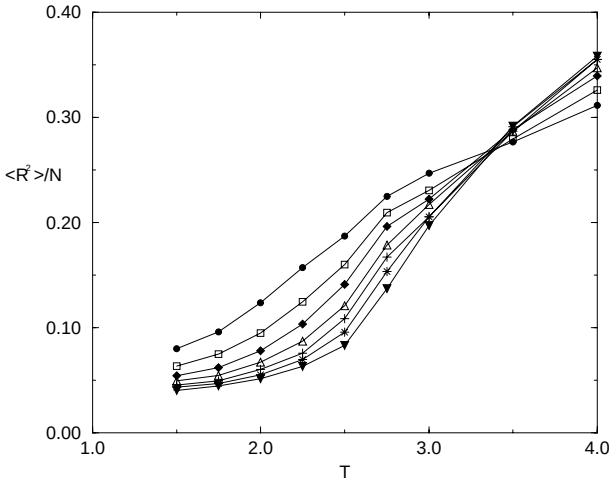

Fig. 15. Search for a second order Θ like transition for $h = 5$: scaled radius of gyration $\langle \frac{R_e^2}{N} \rangle$ *vs.* temperature for $N =$ 100 (•), 150 (□), 200 (♦), 250 (△), 300 (+), 350 (∗), 400 (▼). A crossing occurs for $T \simeq 3.4$.

5 Conclusion

We have seen that ferromagnetic interactions may drive the collapse of a polymer, even in a good solvent. This collapse is very sensitive to the presence of an external magnetic field. It might be possible to design new polymeric magnetic materials, for which the collapse transition is triggered by a magnetic field, at room temperature.

We have also done preliminary simulations on the two-dimensional case (Ising polymer on a square lattice): for $h = 0$, we get a quite abrupt transition around $T_c \sim 1.18$ (which can be compared to the value $T_\theta \simeq 1.5$ [23]). Since the critical dimensions associated with the Θ point (φ^6 theory) and the multicritical G point (φ^8 theory) are respectively $d_\Theta = 3$ and $d_G = \frac{8}{3}$, one expects fluctuations to be important. Further work is needed to elucidate their influence on the mean field phase diagram.

Finally, the present model can be generalized to include

(i) longer range or competing interactions (*e.g.* ANNNI models);
(ii) non Ising local variables ($O(n)$ spins, quadrupoles, ...);
(iii) disorder, either in an annealed (BEG-like [24]) or in a quenched way [25].

References

1. P. Flory, *Principles of Polymer Chemistry* (Cornell University Press, 1953).
2. P.G. de Gennes, J. Phys. France **36**, L55 (1975).
3. E. Pitard, T. Garel, H. Orland, J. Phys. I France **7**, 1201 (1997).

4. A. Coniglio, M. Daoud, J. Phys. A **12**, L259 (1979).
5. G.Z. Archontis, E.I. Shakhnovich, Phys. Rev. E **49**, 3109 (1994).
6. B.K. Chakrabarti, A.C. Maggs, R.B. Stinchcombe, J. Phys. A **18**, L373 (1985).
7. M. Aerstens, C. Vanderzande, J. Phys. A **25**, 735 (1992).
8. J.S. Miller, Adv. Mater. **6**, 322 (1994).
9. A.J. Epstein, J.S. Miller, Mol. Cryst. Liq. Cryst. **228**, 99 (1993).
10. P.G. de Gennes, *Scaling concepts in polymer physics* (Cornell University Press, 1979).
11. J. des Cloizeaux, G. Jannink, *Polymers in Solution, their Modelling and Structure* (Clarendon Press, 1990).
12. A.J. Guttmann, J. Phys. A **22**, 2807 (1989).
13. H. Orland, C. Itzykson, C. De Dominicis, J. Phys. France **46**, L353 (1985).
14. H. Meirovitch, H.A. Lim, J. Chem. Phys. **91**, 2544 (1989).
15. P. Grassberger, R. Hegger, J. Chem. Phys. **102**, 6881 (1995).
16. M.C. Tesi, E.J. Janse van Rensburg, E. Orlandini, S.G. Whittington, J. Stat. Phys. **29**, 2451 (1996).
17. K. Binder, *The Monte Carlo Method in Condensed Matter Physics* (Topics in Applied Physics, Springer, 1995), Vol. 71.
18. E. Orlandini, Monte-Carlo Study of Polymer Systems by Multiple Markov Chain Method, to appear in *Numerical methods for Polymeric Systems*, edited by S. Whittington (IMA Volumes in Mathematics and its Applications, Springer Verlag, 1998).
19. N. Madras, A.D. Sokal, J. Stat. Phys. **47**, 573 (1987).
20. P.H. Verdier, W.H. Stockmayer, J. Chem. Phys. **36**, 227 (1961).
21. P.M. Lam, Phys. Rev. B **36**, 6988 (1987).
22. K. Binder, K. Vollmayr, H.-P. Deutsch, J.D. Reger, M. Scheucher, Int. J. Mod. Phys. C **3**, 1025 (1992), and references therein.
23. P. Grassberger, R. Heeger, J. Phys. I France **5**, 597 (1995).
24. M. Blume, V.J. Emery, R.B. Griffiths, Phys. Rev. A **4**, 1071 (1971).
25. T. Garel, H. Orland, E. Pitard, Protein folding and heteropolymers, in *Spin Glasses and Random Fields*, edited by A.P. Young (World Scientific, Singapore, 1997), pp. 387-443.